Measurement of Thermal Transport in Nb and Nb_3Sn Thin Films by Ultrafast Pump-Probe Thermo-Modulation

1. Introduction

Time-domain thermoreflectance (TDTR) is used for measuring the thermal diffusivity of thin films, including superconducting films [1]. In TDRT, an ultrashort pump laser pulse generates excited carriers, e.g., hot electrons, which then relax by coupling their energy to the phonons. A probe pulse at later times monitors the change either in reflection which can be related to the change in electron (in metals) and lattice temperature. The hot electrons and lattice achieve thermal equilibrium in a time scale of a few picoseconds [2].

The thermal relaxation process involves cooling of hot electrons by transferring their energy to the lattice raising the lattice temperature. The rise in the electron and lattice temperatures, (T_e and T_l) modulates the reflectance *R*. The temporal development of R is used to extract the thermal relaxation of both T_e and T_l [3].

$$\Delta R = a\Delta T_e + b\Delta T_l \quad (1)$$

where, *a* and *b* are constants that depend on the photon energy and the complex dielectric function. It is well established that for 300 K < T_e< 700 K, $(\Delta R)_{max}$ and $(\Delta T_e)_{max}$ are proportional to the laser fluence. Since T_e in our experiment lies within that range, the normalized electron temperature change can be deduced from the measured reflectivity-change [4]:

$$\frac{\Delta T_e}{(\Delta T_e)_{max}} = \frac{\Delta R}{(\Delta R)_{max}} \quad (2)$$

2. Experimental setup

The TDTR setup is schematically shown in Fig. 1. A Ti:sapphire oscillator operating at a center wavelength λ = 800 nm, pulse duration τ ~110 fs, and repetition rate of 80 MHz is used as the laser source. The laser beam is split into a pump and a probe beam by a nonpolarizing beam splitter with an intensity ratio of 9:1. The pump pulse energy was ~1.25 nJ. The pump beam passes through an acousto-optic modulator (IntraAction AOM-402AF3) that modulates it at a frequency of 600 kHz. A half-wave plate is used to rotate the polarization of the pump relative to the probe. A parallel hollow retroreflector (MKS/Newport UBBR1-1S) is mounted on a 300 mm long linear-motorized stage (Thorlabs LTS 300), which is used to adjust the time delay between the pump and probe pulses. The minimum delay steps used between the pump and probe was 6.67 fs. A 10X lens (Thorlabs MY10X-803) is used to focus the pump and the probe beams on the sample to a diameter of 20 and 10 μm, respectively.

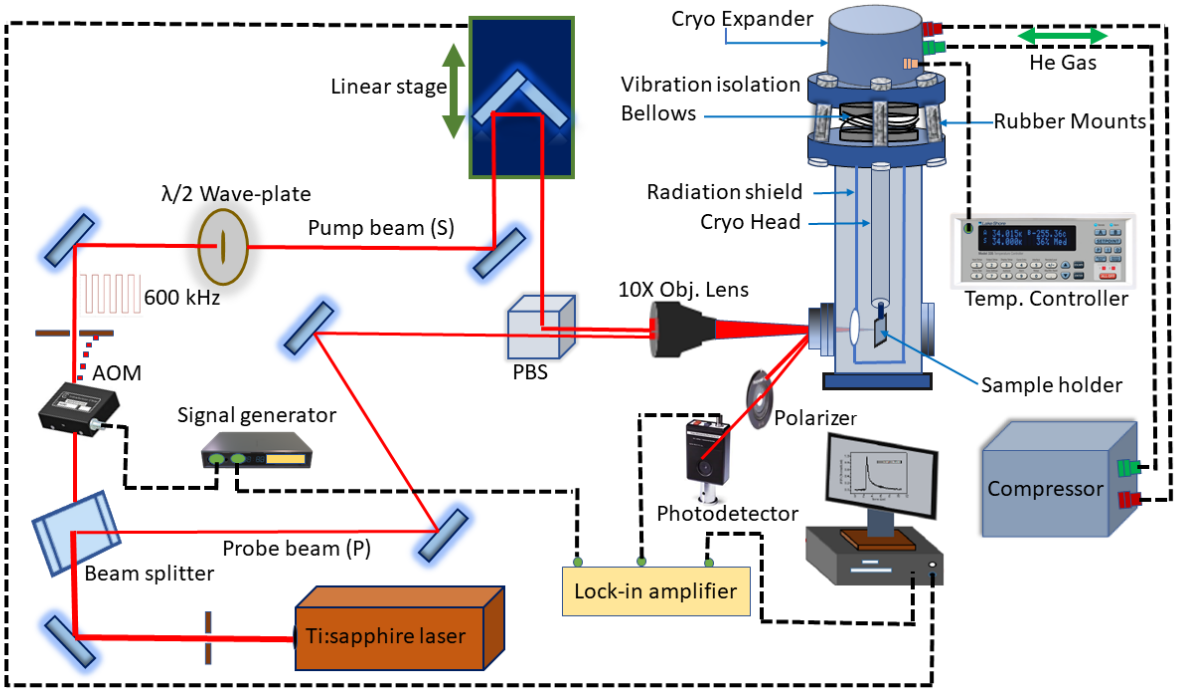

Fig. 1. Femtosecond time domain thermoreflectance pump-probe setup with cryogenic station. An acousto-optic modulator is used to modulate the pump beam at 600 kHz frequency. The linear stage is used to create the time delay between the pump and probe beams. The temperature controller is used to set the temperature at the sample surface inside cryogenic chamber.

Fig. 2. (a) TDTR experiment setup. (b) cryogenic chamber with window access to the sample.

The sample is placed inside the ARS closed-cycle cryocooler that operate on a pneumatically driven Gifford-McMahon (GM) cycle. A temperature controller (Lake Shore 335) is used to set the sample temperature at a desired value. Laser beams enter into the cryogenic chamber through a glass window. The pump beam is incident normal to the sample, while the probe beam is incident at 30^{o} from normal to the sample. The reflected probe beam is detected by a Si photodiode detector (Thorlabs DET 10A). A polarizer is positioned before the detector to block the scattered S-polarized pump beam. A lock-in amplifier (Stanford Research Systems, SR 865A) is used to determine the magnitude and phase of the signal at the modulation frequency of the AOM. A LabView program is used to record $\Delta R(t)$ and control the motion of the linear stage. To determine $\Delta R/R$, ΔR is divided by the static DC signal on the lock-in amplifier from the photodetector in the absence of the pump beam. A photo of the TDTR experiment setup is shown in Fig. 2.

3. Thermal Diffusion in Nb

Niobium films were deposited on copper using AJA ATC Orion 5 Magnetron sputtering system operated in the DC sputter mode with a 2-inch 99.999% Nb sputter target. When the deposition chamber was evacuated to a base pressure of low 10^{-7} Torr the copper substrate was heated to 670 ^{o}C for 30 minutes before starting the deposition. The deposition was performed at 3 mTorr 99.999% pure Ar with a flow rate of 20 SCCM. During sputtering, the DC power applied to the sputter gun was 130 W and the deposition was done with the substrate at room temperature. To obtain a uniformly coated film, the substrate holder was rotated at 50 rpm throughout the deposition. The deposition rate was 0.5 Å/s, as calibrated by a crystal thickness monitor placed at the substrate location prior to deposition. After film growth, the sample was cooled down to 40 ^{o}C per minute to in order not to create significant stress in the Nb film-Cu substrate interface.

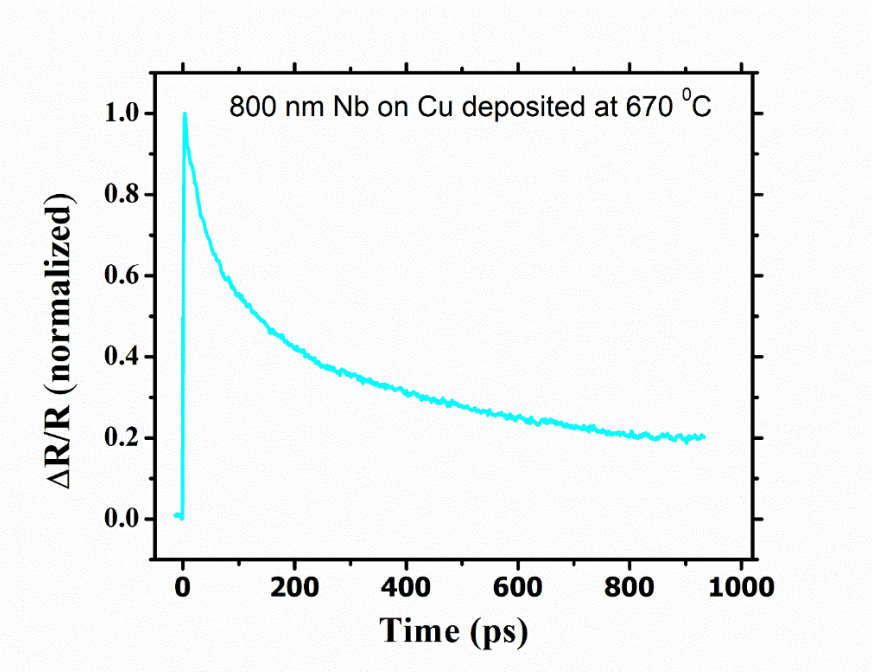

Fig. 3. TDTR data from 800 nm Nb film deposited on copper at 670 ^{0}C.

Fig. 3 shows $\Delta R/R$ from the 800 nm Nb film. The data were taken at room temperature. Unlike the fast decay of a few ps that occurs in highly conductive metals like Cu and Au, in Nb only a slow decay component on the order of ns is observed. Since photon energy of the laser is 1.55 eV and the Fermi energy of Nb is 5.32 eV [5, 6], the smearing of the electron occupancy by ultrafast heating is not observed and the change in reflectance depends more on T_l than on T_e [3].

4. Thermal Diffusion in Nb_3Sn

Nibuim tin (Nb_3Sn) films were also deposited on Nb or sapphire by magnetron sputtering using two different sequential sputtering of Nb and Sn or by co-sputtering. For sequential sputtering, multiple layers of Nb and Sn were deposited on Nb substrates. Both the Nb and Sn targets were 2-inch in diameter. The Nb target was sputtered using a DC magnetron, while the Sn target was sputtered by an RF magnetron. The chamber was evacuated to 10^{-7} Torr before deposition. The deposition was performed at 3 mTorr with an Ar. The deposition was done at room temperature. In sequential sputtering. multiple layers of Nb and Sn with different thicknesses were deposited sequentially with the first layer Sn and the final layer Nb. The final Nb layer minimizes Sn loss during post-deposition annealing. The substrate holder was rotated at 50 rpm throughout the deposition. The as-deposited films were annealed at 950 °C for 3 hours in a different furnace. For depositing co-sputtered Nb_3Sn films the sapphire substrate was heated to 500 ^oC 30 minutes before starting the deposition. The DC and RF power were chosen such that the thickness ratio of Nb and Sn would be 1:0.58 nm. The as-deposited Nb_3Sn film was then annealed at 950 °C for 3 hours.

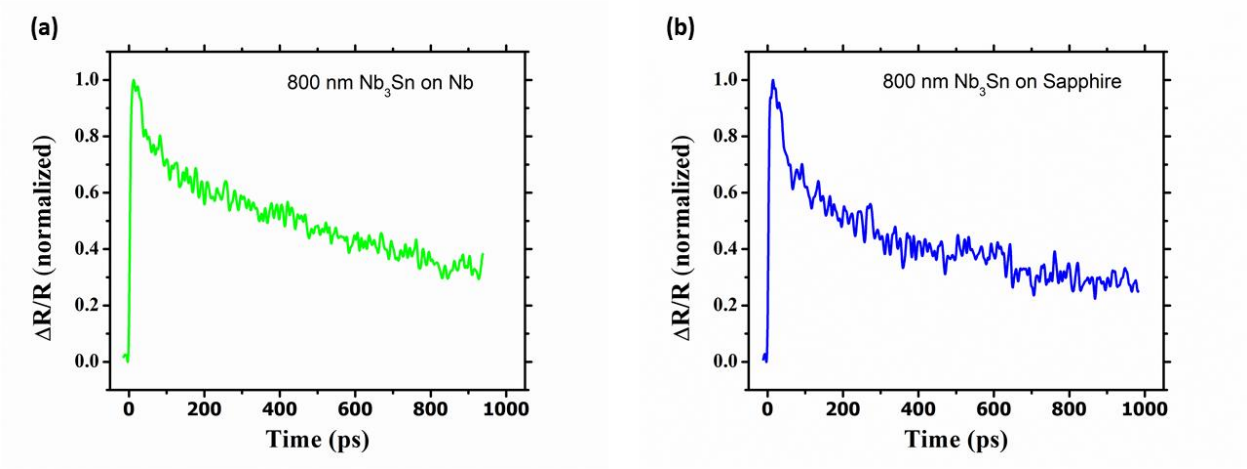

Fig. 4. TDTR from 800 nm Nb_3Sn films (a) Nb_3Sn film deposited on bulk Nb at room temperature using sequential sputtering and (b) Nb_3Sn film deposited on sapphire at 500 °C using co-sputtering of Nb and Sn and annealed at 950 °C for 3 hours

Fig. 4 shows two TDTR scans taken from 800 nm Nb_3Sn samples, one deposited on Nb substrate using sequential sputtering (Fig. 4.a) and the other on sapphire using co-sputtering (Fig. 4.b). Slower decay for Nb_3Sn compared to Nb is observed and the decay time for Nb_3Sn was 490

ps, which is almost twice that of Nb which was 255 ps, as shown in Fig. 5. The slower decay is due to lower thermal conductivity of Nb_3Sn compared to Nb.

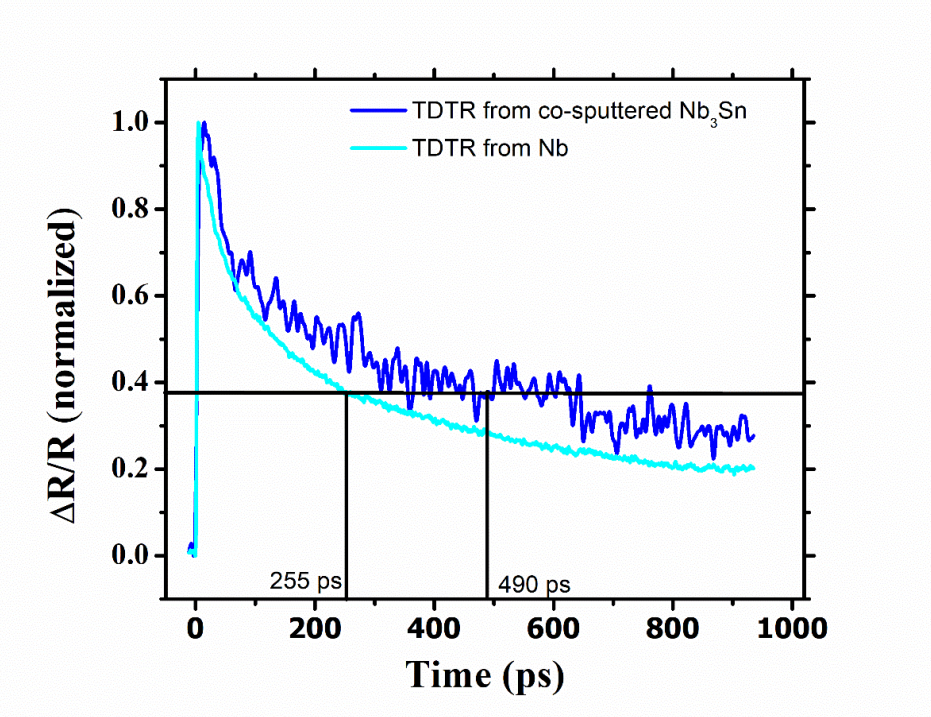

Fig. 5. TDTR curves showing the decay time for Nb and Nb_3Sn.

5. Measurement of Thermal Conductivity

To determine the thermal conductivity *k* of the Nb and the Nb_3Sn films, the *ΔR/R* scans are fitted to the surface temperature from a 1D heat diffusion mode. The 1D approximation is valid because the laser spot size diameter on the surface is much larger than the laser skin depth in Nb.

5.1. Heat Diffusion Model

The one-dimensional heat diffusion model can be used to measure the thermal conductivity since the laser beam focal diameter (20 μm) is large compared to the optical skin depth (20 nm for Nb) [1]. In the conventional Fourier Heat Conduction Model, the radiation energy is assumed to be converted into lattice energy instantaneously and energy transfer in solids is assumed entirely to be a diffusion process [7]. The parabolic one-step heat transfer model deduced from Fourier's law is given by Equation (3).

$$C\frac{\partial T_{(x,t)}}{\partial t} = -k\frac{\partial^2 T_{(x,t)}}{\partial x^2}) + S(x,t) \qquad (3)$$

Where, *T(x,t)* is the temperature profile, *x* is the distance normal to the film surface, *C* is the heat capacity per unit volume, *k* is the thermal conductivity and $S(x,t)$ is the laser source term, heat energy generated per unit volume per unit time. The laser source term has an exponential decay in space to account for absorption and has a Gaussian shape in time. Neglecting the

temperature dependence of the optical properties an approximation of the source term is given by Equation (4) [8, 9].

$$S(x,t) = (1-R)\frac{J}{t_p d} * \exp\left[-\frac{x}{d} - 2.77\left(\frac{t}{t_p}\right)^2\right] \quad (4)$$

Where, R is the reflectivity of the material, J is laser fluence, d is radiation penetration depth and t_p is pulse width. Here R and d are material properties and J and t_p are laser parameters. Lattice heat capacity, thermal conductivity and radiation penetration depth for bulk Nb as reported in literature are 2.3 x 10^{-6} $Jm^{-3}K^{-1}$, 55 $Wm^{-1}K^{-1}$, and 20 nm, respectively [2, 5]. The mass density, specific heat capacity and thermal conductivity for Nb_3Sn at room temperature are 5400 kgm^{-3}, 250 $Jkg^{-1}K^{-1}$, and 1.5 $Wm^{-1}K^{-1}$, respectively [10, 11]. The lattice heat capacity of Nb_3Sn is 1.35 x 10^6 $Jm^{-3}K^{-1}$. The reflectivity R = 0.9 is measured for the 1-μm thick Nb sample deposited on sapphire. The sample was placed at a small angle (15^o) to the incident laser beams and an optical lens was used to collect the whole laser beam reflected from the sample and focus it onto a photodiode detector. The initial temperature is set to the room temperature (300 K).

During the short period of laser heating, heat losses from the front and back surfaces of the film can be neglected, leading to the thermal-insulation boundary conditions:

$$\left.\frac{\partial T}{\partial x}\right|_{x=0} = \left.\frac{\partial T}{\partial x}\right|_{x=L} = 0 \quad (5)$$

5.2. Measuring Thermal Conductivity in Nb

Thermal conductivity is measured by using a MATLAB program for fitting the experimentally obtained thermal response with the temperature profile derived from 1D heat diffusion model for the value of k. Since ΔR is proportional to the temperature, a multiplication factor is needed which is determined by the same MATLAB program by calculating the average of the ratio of the experimental $\Delta R/R$ to fit at multiple times. The goodness of fit is measured by calculating both the root-mean-square error (RMSE) and the coefficient of determination, (R-squared measure). During the first few picoseconds after laser absorption, lattice temperature is small and does not play significant role. Therefore, thermal conductivity should be measured by fitting the experimental data with the theoretical heat conduction model after first few picoseconds.

Figure 6 shows the thermal response from Nb films over 0-935 ps with temporal resolution of 0.667 ps and the fit of this data with 1D heat diffusion model. All data were averaging over 5 scans and no filtering was done. The thermal conductivity for the 800 nm film was 54.5 $Wm^{-1}K^{-1}$ similar to that reported for bulk Nb [5].

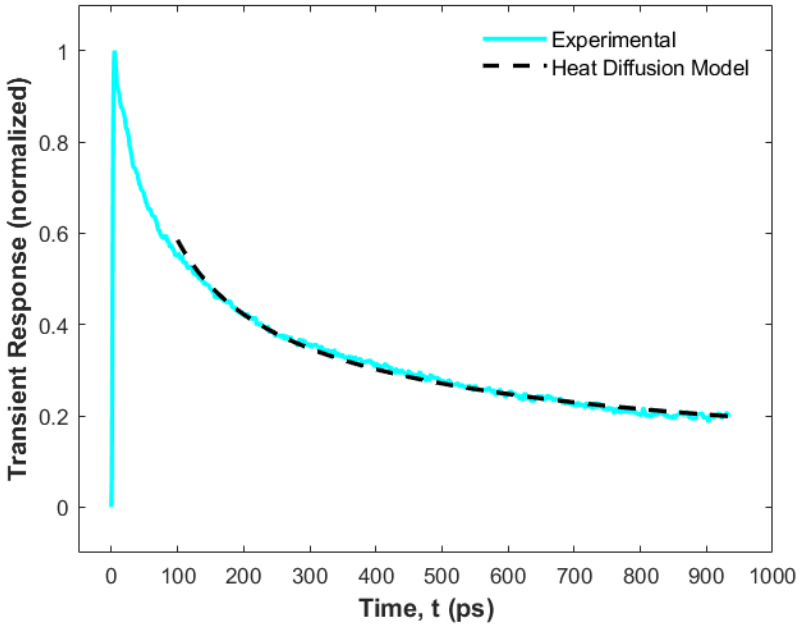

Fig. 6. TDTR from 800 nm Nb film fitted with 1D heat diffusion model gives *k* of 54.5 $Wm^{-1}K^{-1}$.

5.3. Measuring Thermal Conductivity of Nb_3Sn

Using femtosecond TDTR technique it is possible to estimate *k* of Nb_3Sn. Figure 7 shows the TDRT scan for 800 nm Nb_3Sn film on sapphire fitted with 1D heat diffusion model, which gives k = 2.0 ± 0.4 $Wm^{-1}K^{-1}$ at room temperature compared to 1.5 $Wm^{-1}K^{-1}$ reported at room temperature and 2.00 $Wm^{-1}K^{-1}$ reported at 20 K for polycrystalline Nb_3Sn [11].

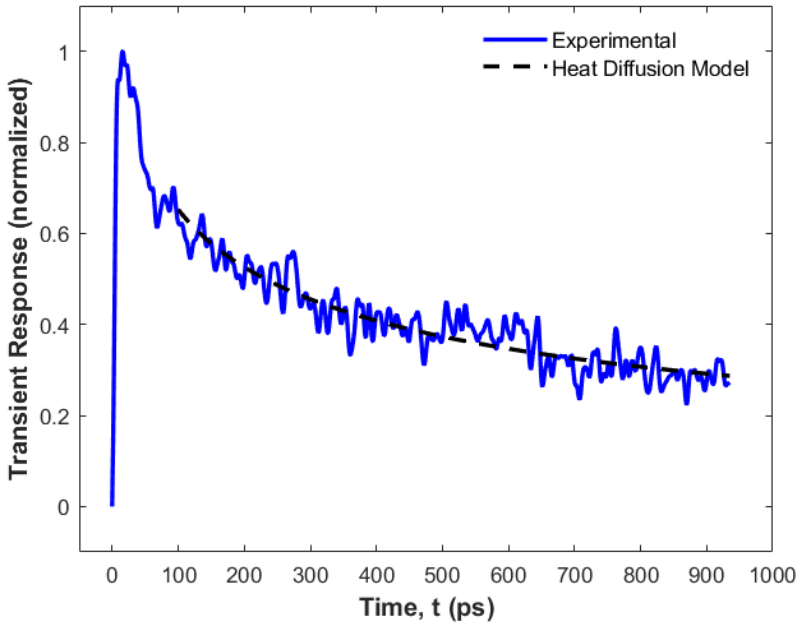

Fig. 7. TDTR from 800 nm Nb_3Sn film fitted with 1D heat diffusion model gives *k* = 2.0 $Wm^{-1}K^{-1}$.

6. Present Status of the Experimental Measurement

We recently installed a cryogenic cooled at pump-probe experiment to measure *k* at temperatures down to less than 9 K. TDTR scans were obtained for 800 nm Nb film at room temperature, 250, and 200 K. *ΔR/R* increases as the sample temperature is reduced, as shown in Figure 8. We are planning to measure thermal conductivity of Nb_3Sn these samples at low temperatures.

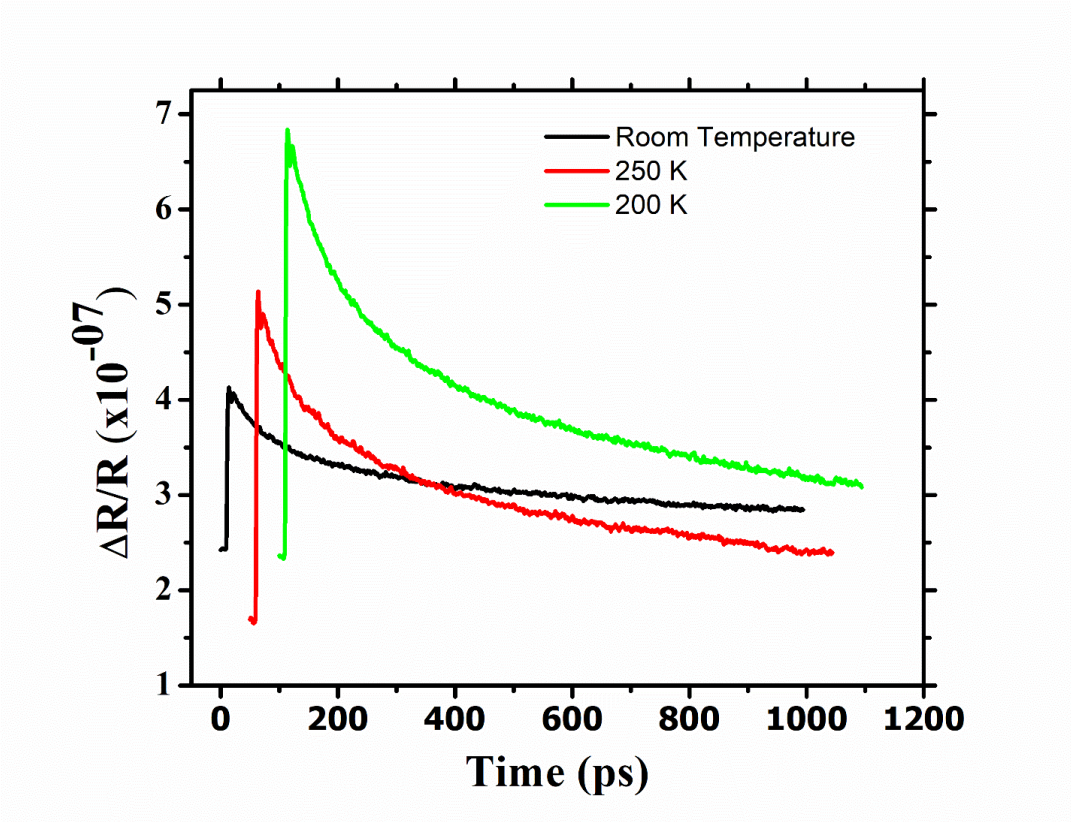

Fig. 8. TDTR obtained from 800 nm Nb on Cu substrate at room temperature, 250, 200 K. The data for the red and green curves are shifted by 50 and 100 ps, respectively.

References

1. R. Cheaito, J. C. Duda, T. E. Beechem, D. L. Medlin, K. Hattar, E. S. Peikos, A. Misra, J. K. Baldwin, P. E. Hopkins, “The effect of ballistic electron transport on copper-niobium thermal interface conductance,” in Proc. ASME Summer Heat Transfer Conference (HT2013), Minnesota, USA, Jul. 2013, pp. 1-5.
2. K.M. Yoo, X.M. Zhao, M. Siddique, R.R. Alfano, D.P. Osterman, M. Radparvar, J. Cunniff, Femtosecond thermal modulation measurements of electron-phonon relaxation in niobium, Appl. Phys. Lett., 56 (1990) 1908-1910.
3. J. L. Hostetler, A. N. Smith, D. M. Czajkowsky, and P. M. Norris, Measurement of the electron-phonon coupling factor dependence on film thickness and grain size in Au, Cr, and Al, Appl. Opt., 38 (1999) 3614-3620.
4. W. M. Roach, D. B. Beringer, J.R. Skuza, W. A. Oliver, C. Clavero, C. E. Reece, R. A. Lukaszew, Niobium thin film deposition studies on copper surfaces for superconducting radio frequency cavity applications, PHYSICAL REVIEW SPECIAL TOPICS - ACCELERATORS AND BEAMS 15, (2012) 062002.
5. M. Mihailidi, Q. Xing, K.M. Yoo, R.R. Alfano, Electron-phonon relaxation dynamics of niobium metal as a function of temperature, Phys. Rev. B, 49 (1994) 3207-3212.
6. N. W. Ashcroft and N. D. Mermin, Solid State Physics, Saunders, 1976.
7. T. Q. QIU, T. JUHASZ, C. SUAREZ, W. E. BRONS and C. L. TIEN, Femtosecond laser heating of multi-layer metals-II. Experiments, Int. J. Heat Mars Trans, 37 (1994) 2799-2808.
8. T. Q. Qiu and C. L. Tien, Heat Transfer Mechanism During Short-Pulse Laser Heating on Metals, Int. J. Heat Mass Transfer, 35 (1992) 719-725.
9. J.K. Chen, J.E. Beraun, Numerical study of ultrashort laser pulse interactions with metal films, Numer. Heat Transfer A, 40 (2001) 1–20.
10. J. Hohlfeld, S. S. Wellershoff, J. Gudde, U. Conrad, V. Jahnke, and E. Matthias, Electron and Lattice Dynamics Following Optical Excitation of Metals, Chemical Phys., 251 (2000) 237-258.
11. L. Rossi, M. Sorbi: CARE-Note-2005-018-HHH "MATPRO: A Computer Library of Material Property at Cryogenic Temperature.", January 16, 2006. Superconductors Database beta http://sdb-server.cern.ch/mediawiki/index.php/Category:Materials.
12. P. Bauer, H. Rajainmaki, E. Salpietro "4. EFDA Material Data Compilation for Superconductor Simulation" EFDA CSU, Garching, 2007.